DYNAMICS AND NON-THERMAL EMISSION OF SHELL SUPERNOVA REMNANTS

S. P. Reynolds
North Carolina State University
Box 8202, Raleigh, NC 27606, U.S.A.
STEVE_REYNOLDS@NCSU.EDU

Abstract

Supernova remnants illustrate the return of mass and energy from stars to the interstellar medium, connecting one generation of star formation with the next. Recent advances in radio and X-ray observational capabilities allow the study of remnants to cast light on these processes. In addition, such studies can be important in understanding the progenitors of Type Ia supernovae, and the core-collapse supernovae apparently associated with γ-ray bursts. I shall review briefly some advances in studies of the dynamics of supernova remnants, with an emphasis on multidimensional simulations, and the implications for radio and X-ray observations. I shall then describe the applications of shock acceleration theory in the context of remnants, focusing on synchrotron emission from radio through X-ray bands, and what it can tell us about the nature of remnants and the physics of particle acceleration.

1 Introduction

Both theory and observation have driven recent advances in our understanding of supernova remnant physics and astrophysics, while the development of other astrophysical areas has come to involve supernovae and their remnants. In this review, I shall focus on two areas of supernova-remnant (SNR) studies that have seen significant advances in the last few years. First, I shall describe improvements in our understanding of global SNR dynamics, partly based on recent hydrodynamic simulations, and then I shall describe advances in observations and theory of shock acceleration. While the basic theory of particle acceleration in strong shocks is now over 20 years old, the discovery of X-ray synchrotron emission from shell remnants has brought new observational information to bear. I shall describe some particular applications of shock-acceleration theory, to remnants SN 1006, RCW86, and G347.3$-$0.5, to illustrate the type of modeling now being done to extract new information and constraints on the theory of particle acceleration in shocks, particularly of electrons. Finally, I shall outline some important questions now confronting us in this area of research. More development of theory of particle injection, of nonlinear shock modification, and of amplification of magnetic field will be required. Models need to be made available as much as possible to the observing community in a form that can be directly compared with data. Observations of spectral curvature in radio should be attempted. X-ray studies separating thermal and non-thermal emission, using the best available models, need to be conducted. X-ray polarimetry may be a new source of important information on magnetic-field strength and geometry in young supernova remnants.

2 Big questions

Supernovae and supernova remnants continue to pose major astrophysical questions. These can be crudely separated into primarily thermal, and primarily non-thermal, issues. In the former category we find questions of supernova energies, types, and nucleosynthetic yields. Major uncertainties still attend our ideas on detailed progenitor mechanisms. While we all agree that Type Ia supernovae are some kind of exploding white dwarf, is the explosion mechanism accretion from an evolved companion (single-degenerate) or merging of two white dwarfs (double degenerate)? Is the explosion a detonation (supersonic), deflagration (subsonic), or initially subsonic with transition to supersonic? Does ignition occur at the center or off center? Given the intense interest focused on cosmological re-

sults derived from supernovae (SNe) Ia as standard candles, this broad uncertainty in the detailed mechanisms seems troubling. Remnants can conceivably begin to cast light on the Ia mechanism (see, for instance, Badenes et al. 2003). The problems attending models of core-collapse supernovae are well-known: all one-dimensional, and even some two-dimensional, simulations fail to explode. At the same time, interest in γ-ray bursts as possible results of extremely asymmetric supernovae has focused new attention on modeling core-collapse supernovae, and on the possibility of extracting information about the asymmetry of the initial event from remnants even thousands or tens of thousands of years old.

Supernova remnants also form excellent theaters for the display of a range of phenomena associated with strong-shock physics. A great deal is still not known observationally about particle acceleration. What fraction of shock energy ultimately goes into fast protons and electrons? How does that efficiency depend on shock Mach number, magnetic field strength or geometry, or other parameters? What energies are reached by electrons and by ions? What is the nature of turbulence and diffusion in both upstream and downstream media? Is magnetic field strongly amplified by some instability, or merely compressed? To what extent does "stochastic" or second-order Fermi acceleration in downstream turbulence compete with first-order Fermi (diffusive shock) acceleration in creating nonthermal particle distributions? Given that supersonic phenomena and strong shocks are ubiquitous in astrophysics, supernova remnants can provide an important laboratory for the study of phenomena with applications across the Universe.

A few big questions are beginning to receive answers from SNR studies.

Maximum particle energies. Electrons with energies of order 200 TeV have been detected in SN1006 (but the spectrum has steepened below the extrapolation from radio wavelengths). There is no evidence yet on maximum energies of ions.

Origin of cosmic rays below the "knee" (10^{15} eV). Plenty of energy from supernovae is available, and we certainly all still believe the bulk of these cosmic rays originate in supernova remnants, but we should perhaps be given pause by the result that in all SNRs studied so far, the electron spectrum currently present in the remnant steepens well short of the "knee" energy (Reynolds & Keohane, 1999; Hendrick & Reynolds, 2001). While cosmic rays at Earth up to the knee are entirely ions (the direct cosmic-ray electron spectrum is already steeper at 1 TeV than the ion spectrum; see references in Blandford & Eichler 1987), ions and electrons, once fully relativistic, should see the Fermi mechanism the same way. Unless radiative losses (the one mechanism singling out electrons) steepen the electron spectrum in every observed SNR, there may be some problem with the origin of Galactic cosmic rays.

Do reverse shocks accelerate particles? In remnants young enough that ejecta are still a non-negligible fraction of the shocked mass, the reverse shock that decelerates them should still be detectable. Might it accelerate particles? While obvious reverse shock structures are not apparent in radio images of any remnant, there is some evidence that in the $\sim 10^4$-year-old remnant RCW86, a reverse shock (identified by excess iron in its spectrum) accelerates electrons to tens of TeV (identified by synchrotron X-rays, Rho et al., 2002).

3 Diagnostics from radio and X-ray observations

Radio observations were historically the earliest to provide systematic discovery and characterization of SNRs, and most SNRs are still radio objects. Radio observations in most cases can locate the shock more effectively than X-rays (e.g., thermal composites; Rho & Petre 1998; also note the radio extension of the SW corner in Fig. 1 beyond X-rays). Polarization observations can in principle provide information on the degree of disorder of the magnetic field and the orientation of the ordered component, but in practice such observations can be highly compromised by effects such as line-of-sight Faraday depolarization, beam depolarization (finite resolution blurring small-scale irregularities), and bandwidth depolarization. If the Faraday depth of a remnant is not small (i.e., expected back-to-front Faraday rotation is not considerably less than a radian), results of polarization observations can be very misleading, even if corrected for foreground Faraday rotation. Significant depolarization between frequencies (smaller polarized fraction at lower frequencies) almost always indicates a cause for concern. However, some broad results are almost certainly correct: young remnants have low polarized fractions, probably due to intrinsic disorder in the magnetic field;

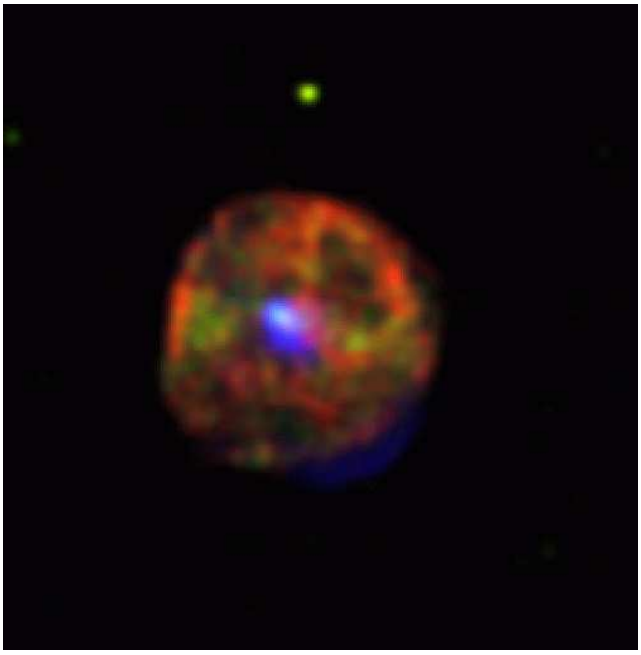

Figure 1: A supernova remnant in the Large Magellanic Cloud, B0453−685 (Gaensler et al. 2003). Blue: 1.4 GHz (Australia Telescope); red, 0.2–0.8 keV (*Chandra*); green, 0.8–2.0 keV (*Chandra*). A central pulsar-wind nebula is visible in both images.

their ordered components are dominantly radial in orientation; older remnants have more varied geometries with occasionally much higher polarized fractions. Finally, radio halos (faint emission ahead of the shock), or their absence, can constrain the extent to which electrons diffuse upstream in the course of Fermi acceleration (Achterberg, Blandford & Reynolds, 1994).

Radio spectroscopy can also provide useful information on young SNRs. The basic synchrotron continuum spectral index α ($S_\nu \propto \nu^{-\alpha}$) gives the slope $s = 2\alpha - 1$ of the electron energy distribution $N(E)$ at the appropriate energies. (We should remember that a frequency range ν_h/ν_l corresponds only to an electron energy range $E_h/E_l = (\nu_h/\nu_l)^{1/2}$ rarely more than a factor of 30 at best). For the 200 or so Galactic shell remnants, the distribution of α peaks around 0.55, ranging from 0.3 to 0.8, with typical errors of order ± 0.05 (Green, 2004). Test-particle shock acceleration theory (see below) predicts that for all but the weakest shocks (Mach numbers $\mathcal{M} \lesssim 5$, we should have $\alpha = 0.5$. Steeper spectra could be explained by modified shocks, in which the relatively low-energy electrons observed have a steeper spectrum resulting from scattering relatively short distances in the smoothed shock velocity transition, and seeing smaller velocity jumps (Ellison & Reynolds, 1991). Flatter spectra could result from confusion with thermal emission, or from a fundamentally different process, such as stochastic acceleration. One prediction of the modified-shock explanation is that the spectrum should be flattening to higher energies (concave up); there is some evidence for this in the radio spectra of Tycho's and Kepler's supernova remnants (Reynolds & Ellison, 1992). Better measurements, with smaller errors, of SNR integrated radio fluxes, over as wide a frequency range as possible, could yield a substantial scientific return.

In recent years, some 20 or so Galactic remnants have shown maser emission in the 1720 MHz satellite line of OH, presumably a result of collisional excitation (see Wardle & Yusef-Zadeh 2004 for a recent review). This emission requires thermal-gas densities $\gtrsim 10^5$ cm^{-3}, and so characterizes small dense clumps in these remnants. It is possible to observe circular polarization in these lines, allowing the deduction of sufficiently strong magnetic fields $B \sim 1$ mG. Observational selection effects are obviously a concern; we don't expect the entire remnant interior to be filled with magnetic fields of such strength, but their presence even in localized clumps is still interesting. This phenomenon is generally observed in remnants interacting with molecular clouds (Wardle & Yusef-Zadeh, 2004). Finally, hydrogen recombination lines have been seen in the spectra of a few highly absorbed remnants (see references in Green 2004), indicating the presence of low-density ionized gas along the line of sight.

For most remnants, X-ray emission is a combination of a thermal bremsstrahlung continuum and emission lines from highly ionized species of astrophysically common elements such as C, N, O, Fe, and α-elements Ne, Mg, Si, S, and Ca. X-ray emission thus localizes hot gas (subject to concerns about foreground photoelectric absorption of soft X-rays). For a given remnant, we expect similar post-shock pressure around the shock, $P_2 \sim \rho_1 u_{\rm sh}^2$, so the hottest regions are those with the lowest pre-shock density ρ_1. The analysis of thermal X-ray spectra of young shell supernova remnants is notoriously complex and difficult; just a few complicating issues include possible lack of temperature equilibration between electrons and ions right behind the shock ($T_e \neq T_i$), lack of ionization equilibrium for young shocks (true if the ionization parameter $n_e t < 10^{12}$ cm^{-3} s), and incomplete or inaccurate

atomic data in the codes, especially for less ionized species than He-like. Much analysis is still done using very crude models, such as "NEI" models assuming a plasma suddenly heated to a constant temperature T a time t ago. These are better than the assumption of ionization equilibrium, but except for discrete clouds with shock crossing times much less than the time since they were shocked, better models should be used. Currently available models include plane-shock models allowing for a range of ionization timescales from zero for just-shocked material up to some maximum, in which initial electron and ion temperatures may be specified arbitrarily, and full Sedov models including the temperature, age, and density information in the Sedov profiles for a point explosion in a uniform medium (Borkowski, Lyerly & Reynolds, 2001). Even these models lack much of the important physics required for SNR analysis, so observers should be aware of their limitations.

Quantitative thermal analysis can, in principle, yield gas temperatures (perhaps electron and ion temperatures separately), ionization timescales $n_e t$, emission measures $\propto \int n^2 dV$ allowing the separate inference of densities and shock age, and relative abundances of heavy elements. With all these free parameters, it is remarkable that any remnant spectrum cannot be well fit; it should be remembered that uniqueness of fits is almost impossible to ascertain. Nevertheless, some remnants do seem to require several shock components, stronger temperature gradients, or other modifications.

While radio synchrotron emission carries relatively little information about detailed shock physics, X-ray synchrotron emission can be significantly more useful. Now most remnants do not seem to require a synchrotron component in their X-ray spectra, allowing an upper bound to be placed on the energy to which their electron distributions currently extend (with the radio-inferred slope). This is true because in all known cases, observed (probably thermal) X-rays fall below the extrapolation of the radio spectrum to X-ray photon energies (Reynolds & Keohane, 1999; Hendrick & Reynolds, 2001). Typical upper limits inferred are of order 10–100 TeV, depending weakly on the mean magnetic field.

If synchrotron X-ray emission can be deduced to be present, its morphology should allow the location of shocks quite precisely; radiative losses on the newly accelerated electrons tend to be severe enough that

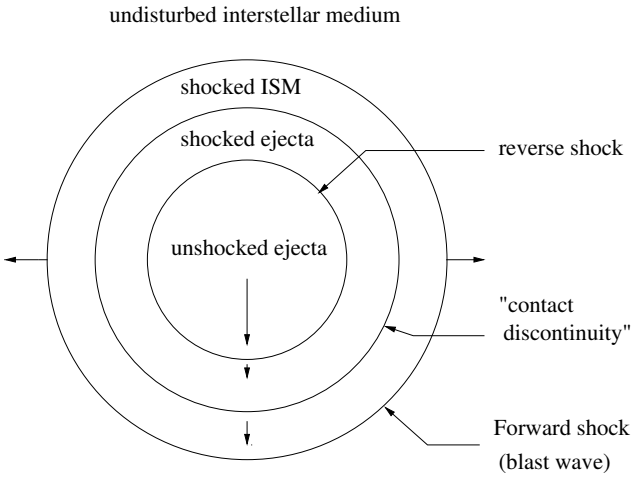

Figure 2: Cartoon of a spherical remnant in the two-shock phase.

such emission should be observable only quite near shocks. Thicknesses of such emission can be used to constrain magnetic-field strengths, if synchrotron losses are responsible (Bamba et al., 2003; Berezhko, Ksenofontov & Völk, 2003). The odd morphology of the hard X-rays, probably synchrotron, from the southwest corner of the remnant RCW86 supports the idea that this is the reverse shock (Rho et al., 2002). The detailed shape of the spectrum, which must be in the process of rolling off since the mean radio-X-ray spectral index of all known remnants is steeper than the radio index, contains information on the maximum electron energies, which themselves encode information on shock properties such as diffusion coefficients, magnetic-field strength, and shock speed. At present, only mean slopes seem possible to differentiate, but models do predict substantially different shapes; models in which electron acceleration is limited by losses have substantially flatter X-ray slopes than those in which it is limited by finite remnant age (or size), or by electron escape (Reynolds, 1998).

4 Dynamical evolution

Recent years have seen significant expansions of the classic four-phase evolutionary scheme of Woltjer (1972): free (undecelerated) expansion of the ejecta until a comparable mass is swept up; a Sedov-Taylor self-similar blast wave phase until the remnant age is comparable to post-shock cooling times; a radiative phase with high-compression, isothermal shocks; and finally, dissipation once the shock velocity drops below

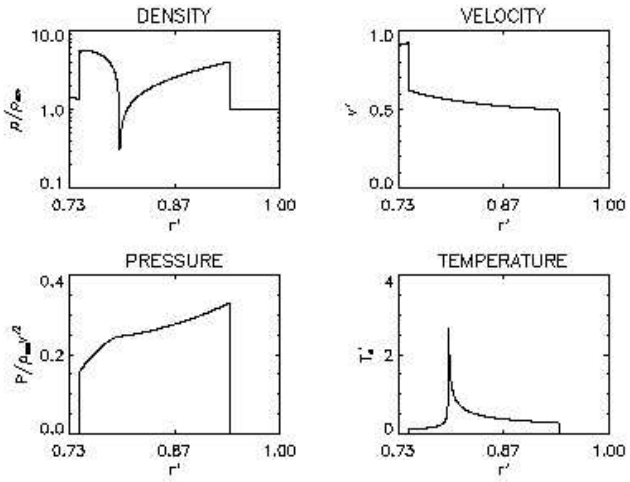

Figure 3: Various quantities for a power-law ejecta density profile (Dwarkadas & Chevalier, 1998).

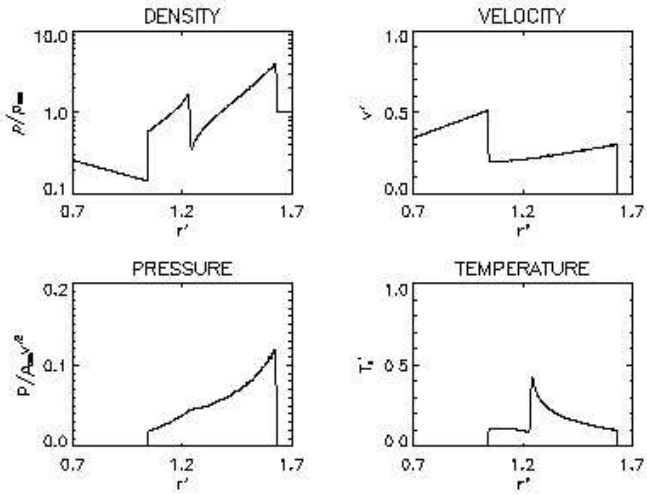

Figure 4: As in the previous figure, for an exponential ejecta density profile (Dwarkadas & Chevalier, 1998).

the ambient sound speed. The most important realization has been that the phases can overlap substantially, and the transitions between phases can last longer than the phases themselves (Cioffi, McKee & Bertschinger, 1988; Blondin et al., 1998). In addition, the idea of undecelerated expansion is clearly naive; after only a few weeks, the ejecta have cooled by adiabatic expansion so substantially that even the very small deceleration required by a minor amount of swept-up matter results in a velocity change greater than the sound speed in the ejecta, i.e., a reverse shock forms, facing inward, decelerating and reheating the ejecta (McKee, 1974). For power-law profiles of ejecta and external density, self-similar two-shock solutions ("self-similar driven waves," SSDW) are possible (Chevalier, 1982a; Nadyozhin, 1985), in which a system of forward and reverse shocks moves out self-similarly, with shocked ambient material and shocked ejecta separated by a "contact discontinuity" across which the pressure is roughly constant (Fig. 2).

For self-similar solutions, all three radii (two shocks and the contact discontinuity) expand as the same power-law of time. If the ambient medium has a density profile $\rho \propto r^{-s}$ and the ejecta have $\rho_{\rm ej} \propto r^{-n}$, then $R \propto t^m$ with $m = (n-3)/(n-s)$. We expect either $s = 0$ (undisturbed ambient medium, appropriate for Type Ia supernovae) or $s = 2$ (constant-velocity stellar wind, appropriate for core-collapse supernovae), while models of Type Ia supernovae typically give $n \sim 7$ and those of core-collapse supernovae give $n \sim 7$–12. Then we expect $m \sim 0.57$ for SNe Ia, and $m \sim 0.8$–0.9 for core-collapse SNe (Chevalier, 1982b). More recent hydrodynamic models of both SN types indicate that power-law density profiles may not be the best approximations; exponential profiles for Type Ia explosions give better descriptions (Dwarkadas & Chevalier, 1998). Figure 3 shows plots of temperature, density, velocity, and pressure for power-law ejecta, while Fig. 4 shows similar plots for exponential ejecta density profiles. Dramatic differences are apparent, for instance note that the ejecta temperature rises steeply behind the reverse shock in the power-law case but drops slightly in the exponential case.

Realistic external density profiles are certain to be more complex than uniform or r^{-2} power-laws. Even in spherical symmetry, the pre-supernova mass-loss phases might involve winds of different speeds and mass-loss rates, for instance a red supergiant wind (slow and dense) followed, as the star's core is exposed, by a blue supergiant wind (much faster but less dense). Shells may result. Interaction of a SNR blast wave with such complex structure will clearly be more involved than these simple solutions suggest.

Of course, spherically symmetric models cannot describe the full range of observed morphologies in SNRs. Multidimensional hydrodynamic simulations show a great diversity of morphologies (Jun, Jones & Norman, 1996; Jun & Jones, 1999; Blondin et al., 1998, 2001). A recent three-dimensional simulation of the distribution of material from the oxygen layers of a 15 $M_\odot$ progenitor after the explosion is shown in Fig.

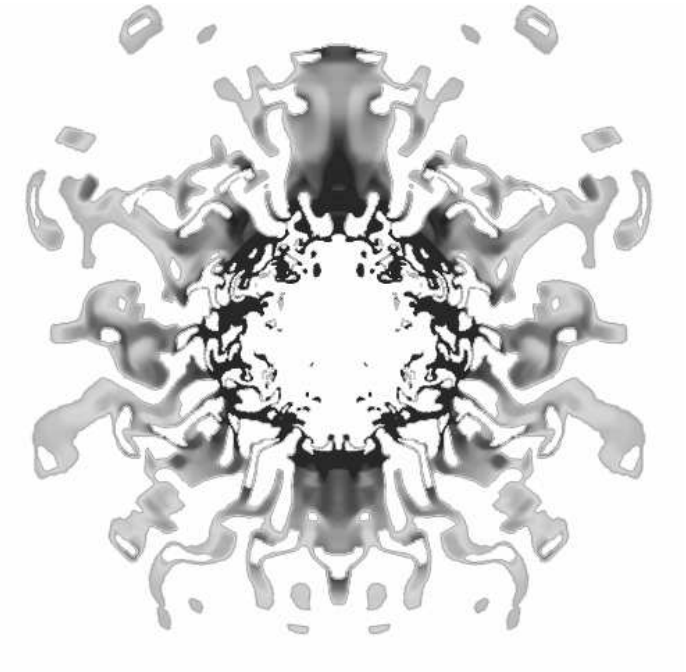

Figure 5: Oxygen distribution in the remnant of a core-collapse supernova. Blondin (private communication).

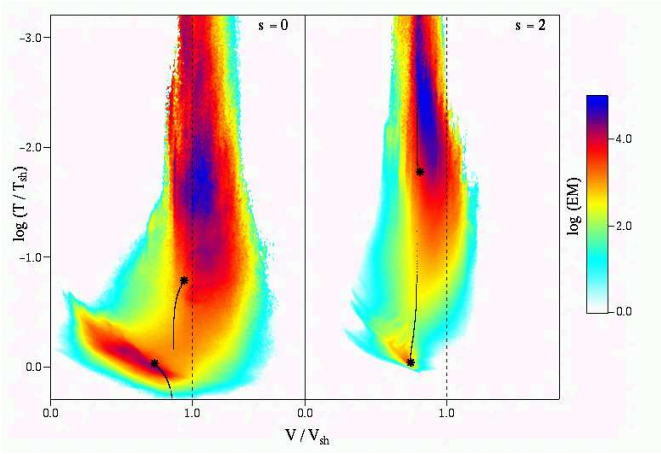

Figure 6: Temperature-velocity plots of emission measure of material behind the forward and reverse shocks in a three-dimensional hydrodynamic simulation of bubbly ejecta (Blondin et al., 2001). Left: constant-density ambient material ($s = 0$). Right: ambient stellar wind ($s = 2$).

5 (J.M. Blondin, private communication).

Additional non-spherical effects can result from inhomogeneous deposition of radioactive ^{56}Ni from a core-collapse explosion, as inferred for SN1987A (Li, McCray & Sunyaev, 1993). In this case, radioactive energy input in clumps of ^{56}Ni will result in their being heated and expanding to form low-density "bubbles." The reverse shock encountering such bubbles can produce dramatically different effects from those found in spherical simulations. Oblique shocks along bubble walls can result in a wide range of ejecta temperatures and post-shock velocities, with higher-velocity (less decelerated) material having lower temperatures, and some material actually moving faster than the contact discontinuity. Interpreting such results will require new forms of contact between observations and models, such as the plots of emission measure versus both temperature and velocity, as shown in Fig. 6 (Blondin et al., 2001).

A well-defined end to early, ejecta-dominated phases is unlikely to occur. While in spherically symmetric models, the reverse shock eventually moves in to the center and disappears, in multi dimensions the reverse shock reflects and bounces in a complex way. Furthermore, the overall deceleration of the outer blast wave takes a long time to complete, so that as much as 10 times the ejected mass may need to be swept up before interior density and velocity profiles begin to resemble those of Sedov self-similar solutions (Cioffi, McKee & Bertschinger, 1988). Recent observations of SNRs in the Magellanic Clouds have turned up several examples of remnants with $M(\mathrm{swept})/M(\mathrm{ejected}) > 10$ in which X-ray emission from ejecta is still prominent (Park et al., 2003; Hendrick, Borkowski & Reynolds, 2003).

Later phases of SNR evolution can be similarly complex. For instance, since cooling times depend on density, remnant interiors will remain hot long after the immediate post-shock gas has had time to cool, resulting in a radiative blast wave with non-negligible interior pressure ("pressure-driven snowplow;" Cioffi et al. 1988). Or different regions around a remnant rim may have different densities, resulting in the blast wave becoming radiative in some regions while remaining adiabatic in others. Such radiative regions may or may not dissipate a significant fraction of the remnant thermal energy, but can have radically different emission properties (bright optical emission, for instance) from parts of the blast wave that remain adiabatic.

5 Particle acceleration

It has been presumed for at least twenty years that the primary mechanism producing fast particles in supernova remnants is the first-order Fermi diffusive shock acceleration (DSA) process (see reviews by Blandford & Eichler [1987], Jones & Ellison [1991], Malkov & Drury [2001], among others). Arguments for this

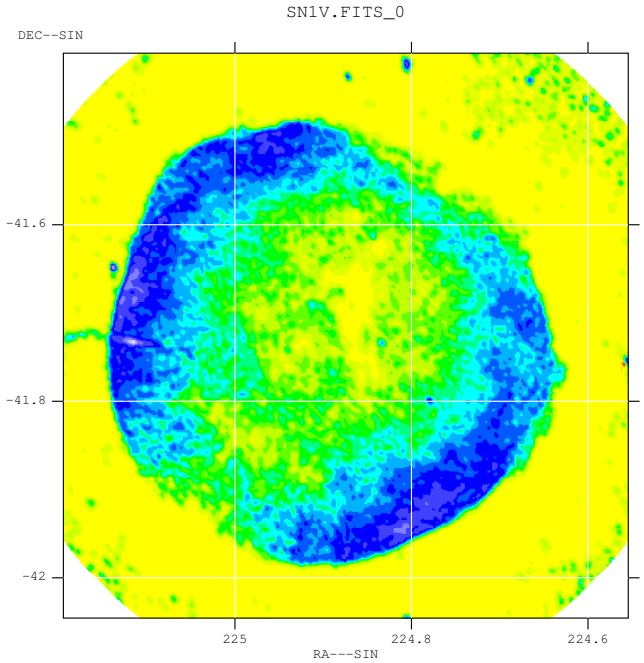

Figure 7: SN1006 at 1370 MHz (Reynolds & Gilmore, 1986). VLA image with resolution of $16'' \times 20''$.

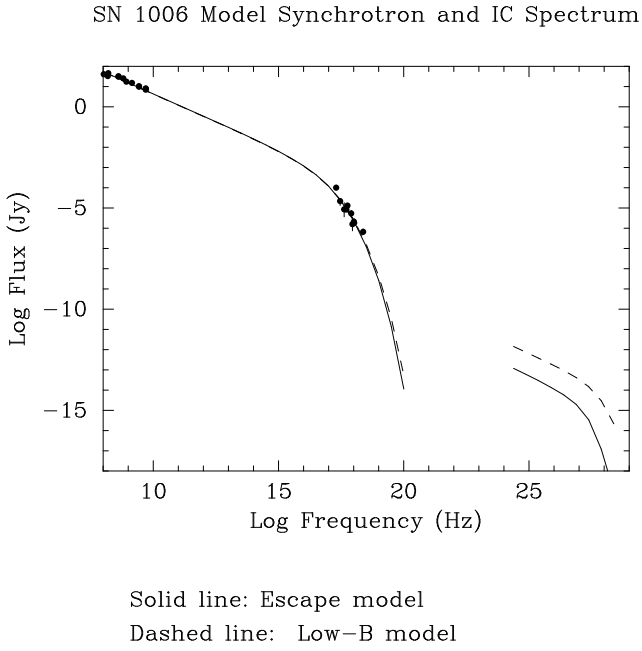

Figure 8: Model for radio to X-ray synchrotron emission from SN1006 (Reynolds, 1996; Dyer et al., 2001). Predicted TeV emission from inverse-Compton upscattering of CMB photons is shown as well.

include the observed spectra of radio-emitting electrons in SNRs, the high brightness of emission in presumably adiabatic, low-compression shock waves, and considerations of detailed spectral shape and energetics (these arguments are summarized in Reynolds [2004a]). While I shall assume that DSA is responsible for non-thermal particle distributions in SNRs, it is important to remember that second-order Fermi (stochastic) acceleration is also expected to operate in the turbulent downstream flows behind shocks. One argument favoring DSA over stochastic acceleration results from comparing the time required to accelerate a particle to a given (extreme-relativistic) energy E:

$$\frac{\tau_I}{\tau_{II}} \sim \left(\frac{u_{\rm sh}}{v_A}\right)^{-2} \qquad (1)$$

where $u_{\rm sh}$ is the shock speed and v_A the Alfvén speed downstream. Since $v_A^2 = B^2/4\pi\rho \sim P_B/P_{\rm gas}$, we normally expect $\tau_I < \tau_{II}$ unless magnetic pressure reaches equipartition with thermal pressure downstream. But the rate of acceleration is not the whole story; in some circumstances, one might expect modification of a particle spectrum due to significant downstream stochastic acceleration. Unfortunately, the predicted stochastic spectrum depends on details of particle diffusion and the spectrum of magnetic turbulence to a much greater extent than DSA, so unique theoretical predictions are difficult.

Even if we accept DSA as the primary mechanism accelerating particles in SNRs, we are left with many questions. Can we identify absolutely unambiguous signs of its operation (rather than simply ruling out competing explanations)? What is the efficiency, typically measured as the fraction of shock energy $\rho u_{\rm sh}^2$ going into fast particles? What about the ratio of energy in ions to that in electrons? Is the efficiency high enough that nonlinear backreaction of accelerated particles on the shock structure must be taken into account? What are observational clues that shocks are nonlinear? How are electrons "injected" into the Fermi mechanism if their initial thermal energies are so low (as expected) that they see the shock initially as smoothly varying gradients instead of as a discontinuity? How does the "obliquity" angle ($\theta_{\rm Bn}$, the angle between the shock normal and upstream magnetic field) affect the injection, diffusion, and acceleration of particles? What are the diffusive properties of upstream and downstream media? Are self-generated MHD waves present? Is the magnetic field strongly amplified in cosmic-ray-dominated shocks, as suggested in recent work (Lucek & Bell, 2000)?

A better understanding of the physics of shock acceleration can help provide substantial astrophysical benefits in the interpretation of SNR observations, allowing, perhaps, more reliable deductions of shock velocities and their history, and the magnetic-field strength and geometry. If synchrotron X-rays are a common component of SNR X-ray spectra, they must be understood even if one's primary interest is in the interpretation of thermal emission, as the presence of a synchrotron continuum, incorrectly interpreted as thermal, can lead to wildly erroneous conclusions.

The basic particle spectrum expected from shock acceleration is approximately a power-law with an exponential cutoff at an energy $E_{\rm max}$ set by one of several possible mechanisms (Reynolds, 1996): radiative losses, escape, or finite remnant age (or size):

$$N(E) = KE^{-s}\exp\left(-E/E_{\rm max}\right). \qquad (2)$$

The nonlinear effects mentioned above can alter the slope of the distribution at lower energies by amounts corresponding to a few tenths in photon energy index $\alpha = (s-1)/2$. Observing radiation from the quasi-power-law part of the spectrum provides information on the electrons only, of course, and the value at the observing frequency can give the shock compression ratio on the scale of the diffusion length of the electrons emitting at that frequency. Unfortunately, without knowledge of the magnetic-field strength, it is difficult to make direct use of this information. The observed intensity fixes the product $KB^{1+\alpha}$, or roughly the product of electron and magnetic-field energy densities; independent information is required to separate those contributions. The assumption of minimum total energy gives roughly equal energies in field and particles, but since one is not sure whether to insist on equipartition between electron energies and magnetic field, or all particle energies with an unknown amount in ions, and since there seems no obvious physical mechanism producing such equipartition, since in any case all non-thermal energies are not likely to exceed a few tenths of the total thermal energy, the assumption of equipartition as a means to estimate magnetic-field strengths is of limited utility.

Considerably more information can be obtained if one observes the cutting-off tail (radiation from electrons with $E \gtrsim E_{\rm max}$. The spectrum from this exponential cutoff is approximately $S_\nu \propto \nu^{(-\sqrt{\nu/\nu_{\rm max}})}$, where $\nu_{\rm max} \propto E_{\rm max}^2 B$, and for each cutoff mechanism, $E_{\rm max}$

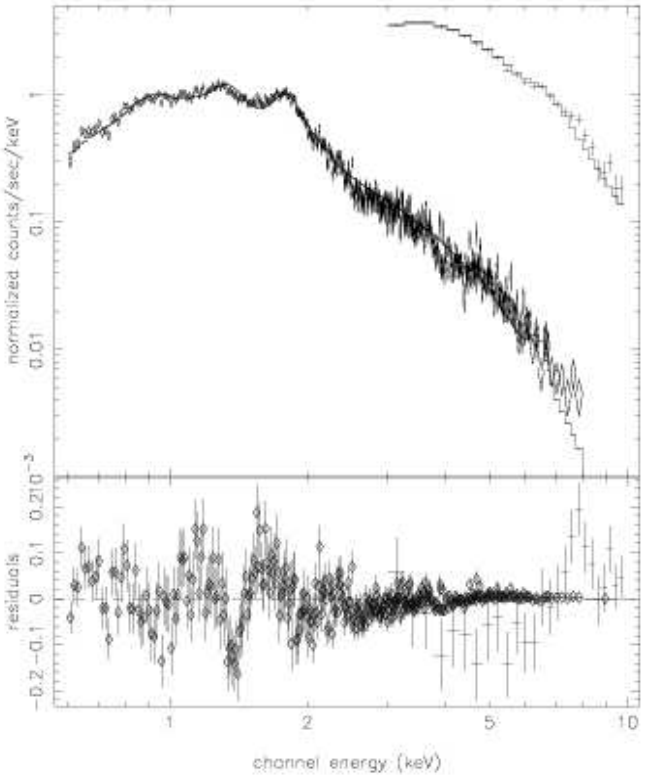

Figure 9: Combined thermal/non-thermal fit to *ASCA* GIS and *RXTE* (upper right) observations of SN1006 (Dyer et al., 2001).

is a different function of diffusion coefficient, shock velocity, remnant age, magnetic field, and shock obliquity. For a real, inhomogeneous remnant, in which different locations on the shock may have different values of $E_{\rm max}$, and where the post-shock electron distribution evolves due to adiabatic and radiative losses, the emergent integrated spectrum will fall off more slowly than the above expression, and the detailed spectral shape contains information about which mechanism is responsible (Reynolds, 1998).

Finite remnant age demands $t_{\rm accel} \lesssim t$, for ions or electrons, implying (Reynolds, 1998)

$$E_{\rm max} \propto \int_{t_i}^{t} B u_{\rm sh}^2 dt \qquad (3)$$

$$\lesssim 100\left(\frac{B}{3\,\mu G}\right)\left(\frac{u_{\rm sh}}{3000\ {\rm kms}^{-1}}\right)^2 t({\rm yr})\ {\rm GeV} \lesssim 100\ {\rm TeV} \qquad (4)$$

Particles may escape the remnant if MHD waves are absent above some wavelength $\lambda_{\rm max}$, resulting in a cutoff for either ions or electrons. The requirement $\lambda_{\rm wave} \sim r_g(E)$ then gives

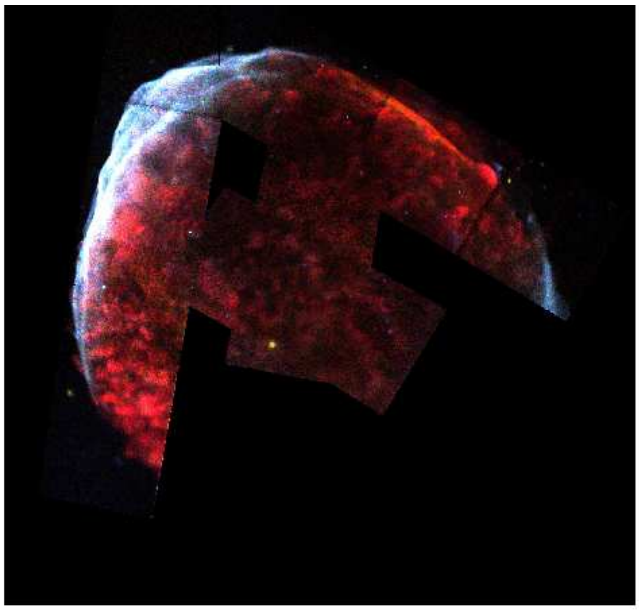

Figure 10: *Chandra* image of SN1006. Red: 0.5–0.8 keV. Blue: 1.2–5 keV.

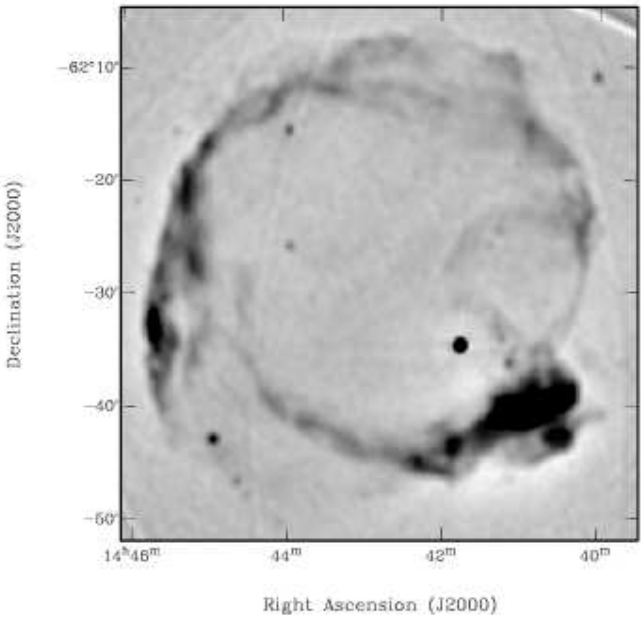

Figure 11: MOST image of RCW86 (Whiteoak & Green, 1996) (843 MHz; 45″ resolution).

$$E_{\rm max} \propto \lambda_{\rm max} B \sim 23 \left(\frac{\lambda_{\rm max}}{10^{17}\ {\rm cm}}\right) \left(\frac{B}{3\ \mu G}\right)\ {\rm TeV} \tag{5}$$

Finally, radiative losses (synchrotron unless $B \lesssim 3\ \mu$G, in which inverse-Compton losses on the cosmic microwave background predominate) require $t_{\rm accel} \lesssim t_{\rm loss}$, producing a cutoff in the electron spectrum above

$$E_{\rm max} \sim 100 \left(\frac{B}{3\ \mu G}\right)^{-1/2} \left(\frac{u_{\rm sh}}{3000\ {\rm kms}^{-1}}\right)\ {\rm TeV}. \tag{6}$$

Electrons with energy E radiate the peak of their synchrotron emission at $\nu_c \propto E^2 B$, so for loss-limited acceleration, $\nu_c \propto u_{\rm sh}^2$, *independent* of B.

All these mechanisms can easily produce values of $E_{\rm max}$ high enough to result in significant synchrotron X-ray emission.

6 X-ray synchrotron emission

The first shell remnant in which X-ray synchrotron emission was proposed was SN1006 (Becker et al., 1980; Reynolds & Chevalier, 1981), a VLA image of which is shown in Fig. 7. Early data and models were both uncertain, but observations with *ASCA* in 1994 (Koyama et al., 1995) showed unmistakably that both thermal emission, from the remnant center, and non-thermal emission, from the bright limbs, were present, leading to more sophisticated models (Reynolds, 1996) (Fig. 8). The integrated *ASCA* GIS spectrum of SN1006 was shown to be well described by a combination of a synchrotron model limiting elec-

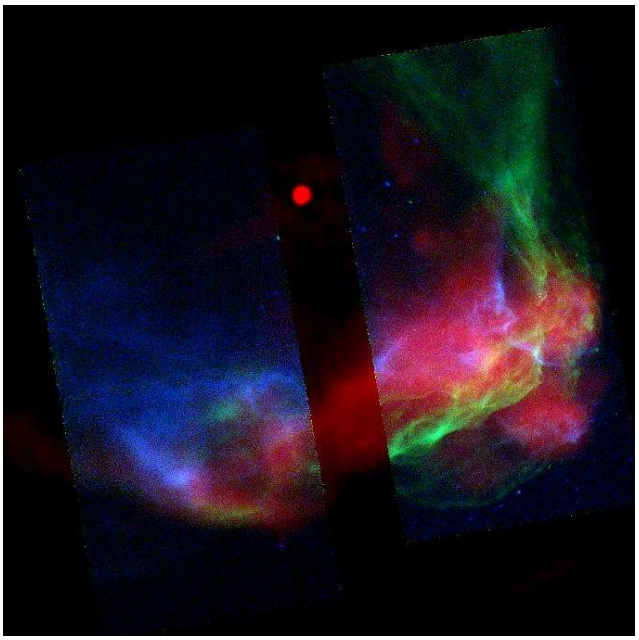

Figure 12: Radio and X-ray image of the southwest corner of RCW86. Radio: Australia Telescope (Dickel, Strom & Milne, 2001); X-ray, *Chandra*: green, 0.5–1 keV; blue, 2–10 keV (Rho et al., 2002).

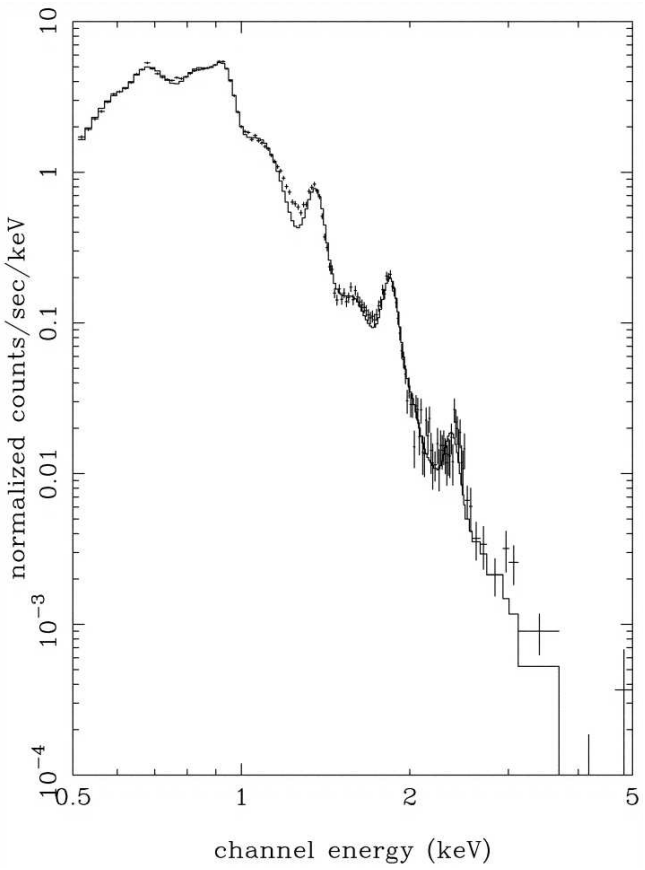

Figure 13: *Chandra* spectrum of a soft X-ray filament in RCW86, fit with a thermal plane shock model (Rho et al., 2002).

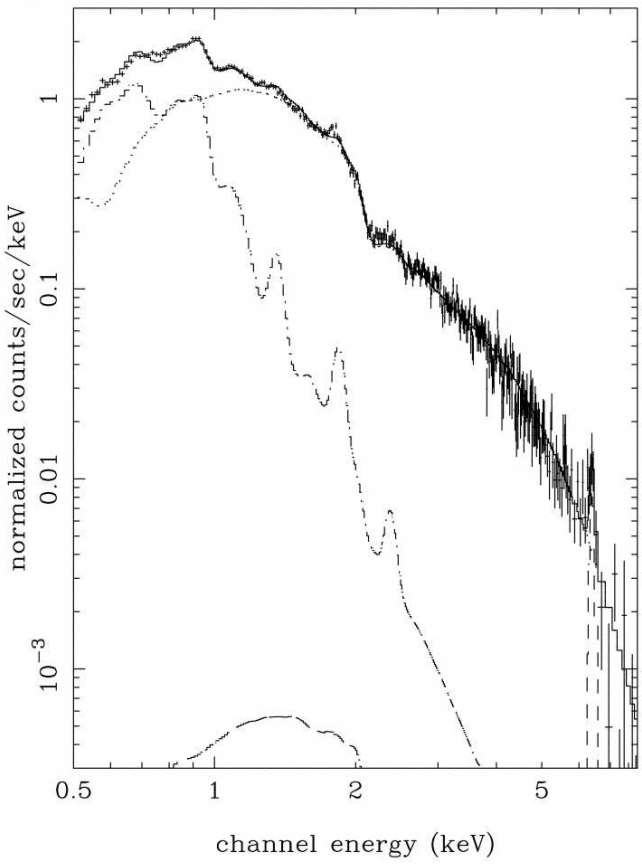

Figure 14: *Chandra* spectrum of a hard X-ray region in RCW86, fit with a synchrotron model (SRCUT) and a thermal plane shock model (Rho et al., 2002).

tron energies by escape, and a thermal plane-shock model with an overabundance of iron (Fig. 9, Dyer et al., 2001). These conclusions were supported by analysis of much higher-resolution images and spectra from *Chandra* (Long et al., 2003, Fig. 10).

If synchrotron X-ray emission can dominate one remnant, and theoretical expectations are that special conditions are not required, then we might expect to see remnants in which synchrotron X-rays are present but not dominant. It is likely that RCW86 (Fig. 11) is such a remnant. The designation "RCW86" actually refers to the bright optical emission from radiative shocks in the southwest of the radio remnant G315.4−2.3. However, that region also shows non-radiative shocks with speeds of 600–900 km s^{-1} (Ghavamian et al., 2001). Its *ASCA* spectrum showed surprisingly weak lines, even of Ne and other elements not likely to be condensed in grains, that were hard to interpret in conventional models (Vink, Kaastra & Bleeker, 1997). However, the addition of a synchrotron continuum allowed a solar-abundance plane-shock model to describe the data well (Borkowski et al., 2001). A later *Chandra* observation (Rho et al., 2002) showed strikingly contrasting morphology of soft (0.5–1 keV) and hard (2–10 keV) X-rays (Fig. 12), with regions dominated by soft emission showing a thermal spectrum (Fig. 13), while hard-spectrum regions showed the weakest lines and hardest continuum, suggesting domination by synchrotron emission (Fig. 14). The additional presence of Fe Kα from such regions suggested that the shocks accelerating the required $\sim$ 10 TeV electrons are moving into material with elevated iron abundance, that is, that these are portions of the reverse shock.

In some locations, the coincidence of a hard X-ray filament with the edge of a radio-emitting region is suggestive of a shock accelerating particles with a range of energies, with the highest-energy electrons surviving only a short time downstream due to radiative losses, while radio-emitting electrons persist much longer (further). A competing explanation of the

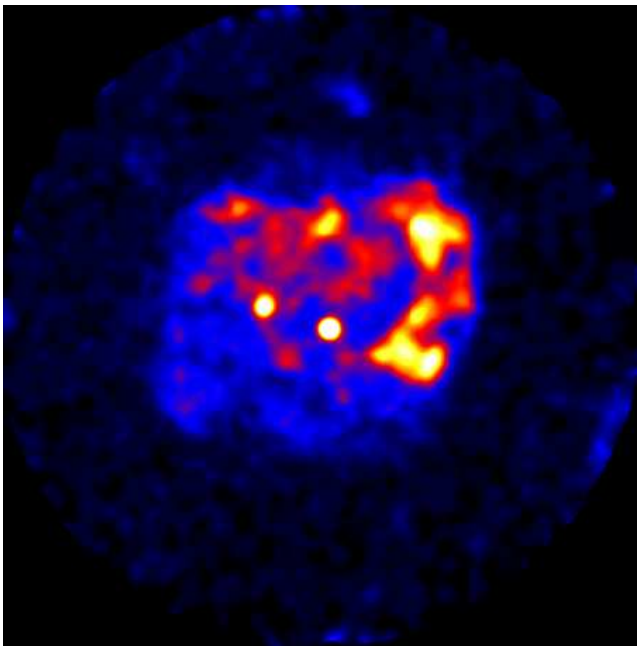

Figure 15: *ROSAT* PSPC mosaic of G347.3−0.5 (Slane et al., 1999).

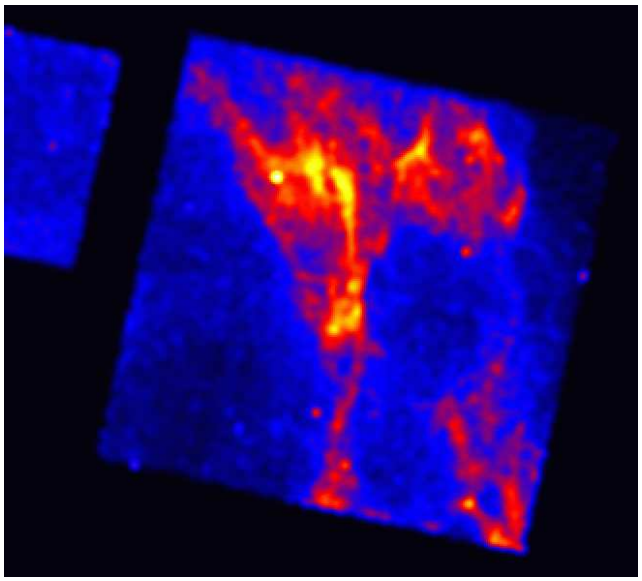

Figure 16: *Chandra* ACIS-I image of northwest corner of G347.5−0.3 (Lazendic et al., 2004).

weak lines and hard continuum invokes non-thermal bremsstrahlung from slightly supra-thermal electrons (Vink et al., 2004), but this interpretation suffers from problems of energetics (Rho et al., 2002).

Two other Galactic remnants show X-ray spectra without statistically significant line features: G266.2−1.2 ("Vela Junior," superposed on the shell of the Vela supernova remnant) and G347.3−0.5 (Fig. 15; Slane et al. 1999). The latter object has a complex morphology; a *Chandra* image of the northwest corner is shown in Fig. 16. This object was reported to have TeV γ-ray emission (Enomoto et al., 2002), and broad-band modeling has been done with a modified-shock model (Ellison, Slane & Gaensler, 2001). More recent modeling, including the results of the above *Chandra* data, found that a synchrotron model for the X-rays, coupled with inverse-Compton upscattering of CMB photons for the TeV emission, could describe the integrated spectrum reasonably well with an electron roll-off energy $E_{\rm max}$ of 5 TeV (Fig. 17). This fit found a reasonable magnetic field strength of 15 μG, but required that it be confined to only about 1% of the volume (Lazendic et al., 2004). This small filling factor may be consistent with the highly filamentary structures seen in Fig. 16, but it is also possible that a different mechanism is required for the TeV γ-rays (Butt et al., 2002). Future observations and modeling of this object will be important in constraining particle acceleration to very high energies.

Detailed modeling of X-ray synchrotron emission from remnants can cast light on shock microphysics as well. For a remnant encountering a uniform upstream magnetic field, the variation in obliquity angle $\theta_{\rm Bn}$ can mean a large difference in acceleration rates between locations of quasi-parallel ($\theta_{\rm Bn} \sim 0^\circ$) and quasi-perpendicular ($\theta_{\rm Bn} \sim 90^\circ$) shocks (Jokipii, 1987). The difference rises as the parallel diffusion coefficient (along the magnetic field) increases. The diffusion coefficient as a function of energy, $\kappa(E)$, is set by the spectrum of MHD waves responsible for scattering the particles: if the wave intensity as a function of wavenumber is $I(k) \propto k^{-n}$, then $\kappa(E) \propto E^\beta$ with $\beta = 2 - n$. Then a particular spectrum (such as Kolmogorov, with $n = 5/3 \Rightarrow \beta = 1/3$, or Kraichnan, with $n = 3/2 \Rightarrow \beta = 1/2$,) makes particular predictions for the morphology of synchrotron X-ray emission. Figure 18 shows predicted images for four assumed energy dependences $\kappa(E) \propto E^{-\beta}$ (Reynolds, 2004b). Since no known remnant shows morphologies like those for values of β significantly lower than 1, it seems likely that the wave spectra near SNR shocks are close to "white noise," $I(k) \propto k^{-1}$, implying equal energy in equal logarithmic intervals. This is the spectrum required to produce "Bohm diffusion" (mean free path equal to gyroradius) at all energies, suggesting that the turbulence in which particles scatter near SNRs

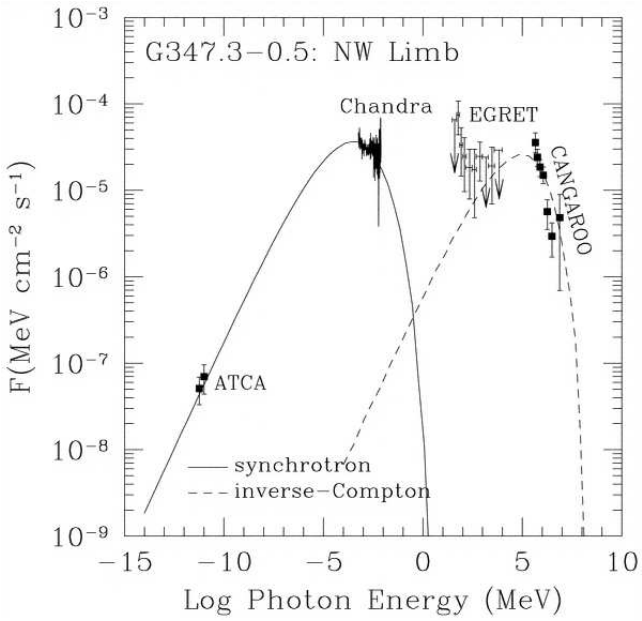

Figure 17: Broadband fit to radio through TeV γ-ray spectrum of G347.3−0.5 (Lazendic et al., 2004).

is self-generated, as held by shock-acceleration theory.

7 X-ray polarimetry

A potentially significant new avenue for observational information on shock acceleration in SNRs is X-ray polarimetry. While a dedicated polarimeter has not been available on an X-ray satellite for many years, a new generation of detector technologies may allow much higher sensitivities in the near future (see proceedings of a workshop on X-ray Polarimetry held at SLAC, February 2004: http://www-conf.slac.stanford.edu/xray_polar/Talks.htm). Such capabilities offer outstanding opportunities in SNR physics. First, we could simply verify that the featureless X-ray continua seen in SN 1006 and a few other remnants really are synchrotron emission, as polarization is the bulletproof evidence. Second, contributions of synchrotron X-rays to mixed spectra as in RCW86 could be identified or verified without requiring extensive, model-dependent spectral analysis. Once detected, polarized X-rays can give information on the orientation and degree of order of the magnetic field, totally unconfused by the Faraday effects that can make radio polarimetry hard to interpret. However, the resolution of any realistic X-ray polarimeter will be considerably poorer than that attainable at radio wavelengths, so judicious combinations of radio and X-ray information will yield optimal results. Once

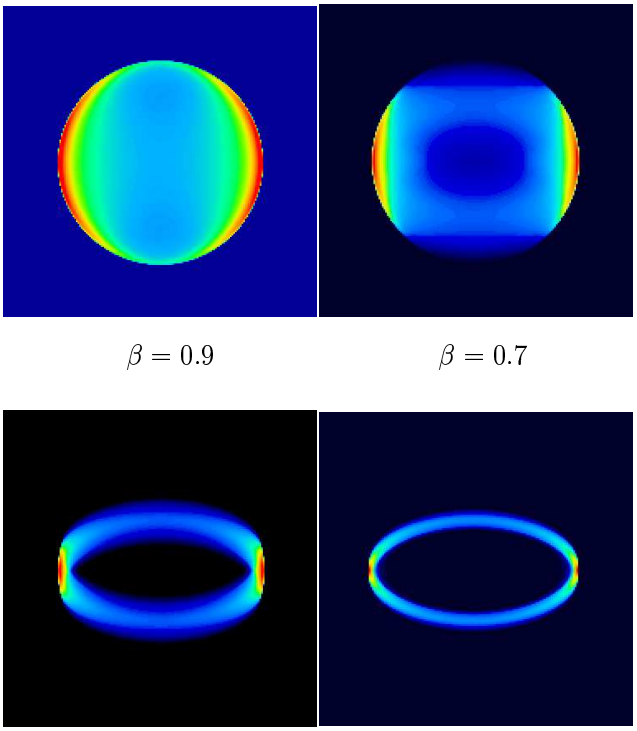

Figure 18: Simulations of X-ray synchrotron morphology (1 keV) for different assumptions about energy dependence of the diffusion coefficient (Reynolds, 2004b).

"true" polarized fractions are obtained from X-ray observations, any reduction in polarization at radio wavelengths is presumably due to Faraday depolarization in the source, giving independent information on the internal electron density and line-of-sight magnetic-field strength. Any successful X-ray polarimeter mission should include SNR physics as a substantial component of its justification.

Examples of simulations of polarized radio and X-ray emission are shown in Fig. 19, 20, 21, and 22. A uniform upstream magnetic field is assumed, with sky-plane projection vertical and aspect angle of 60° with the line of sight. The magnetic field downstream is assumed to evolve by pure flux freezing, with no turbulent amplification or randomization of direction. However, substantial Faraday rotation was produced in the radio (300 MHz) image by assuming a somewhat large upstream magnetic-field strength, B = 30 μG, though in a low-density (n_0 = 0.1 cm^{-3}) medium. The misleading polarization vectors in Fig. 21 illustrate the problems interpreting radio polarimetry.

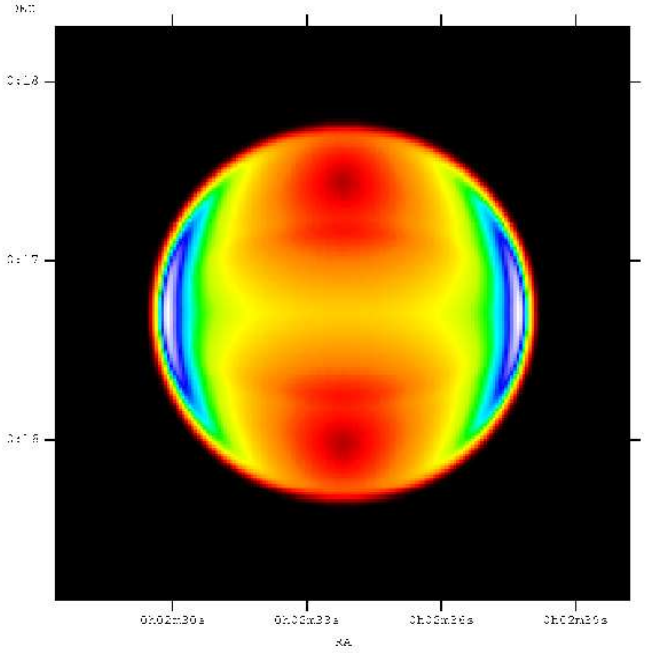

Figure 19: Simulation of 300 MHz synchrotron emission from a Type Ia remnant in the Sedov phase.

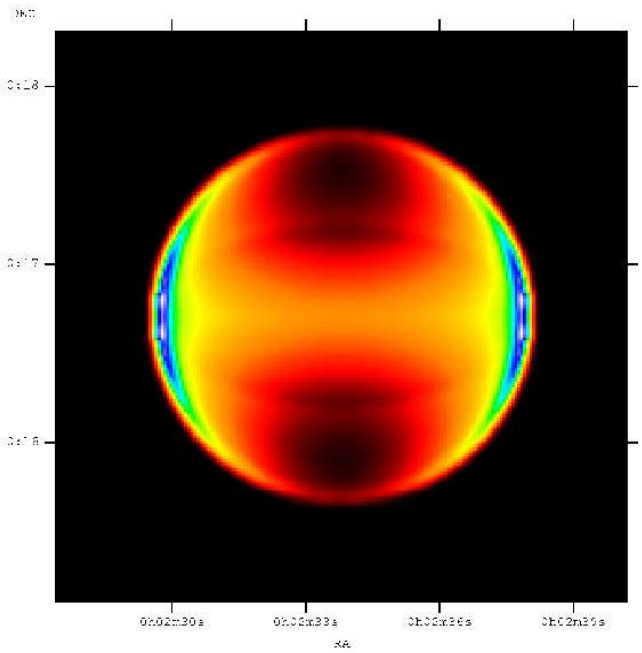

Figure 20: As in Fig. 19, for emission at 1 keV.

8 Summary and future questions

In the last few years, significant new information at radio and X-ray wavelengths has increased our understanding of shell supernova remnants and of particle acceleration.

1. There is still no known shell remnant with unbroken radio-to-X-ray spectrum. All SNR electron spectra begin to steepen below ~ 100 TeV.
2. Simple radio-to-X-ray spectral models of synchrotron emission from an electron distribution $N(E) = KE^{-s}\exp(-E/E_{\rm max})$ (XSPEC: SRCUT) are surprisingly robust when applied to SNRs with synchrotron components.
3. Proper-motion expansion results may differ between radio and X-rays if ejecta are highly inhomogeneous.
4. RCW86 appears to have electron acceleration to TeV energies in reverse shocks. Radio-X-ray morphological comparison supports this.
5. Broad-band fitting (radio to TeV) can produce strong constraints (e.g., small filling factor for **B** in G347.3−0.5).

Of course, major problems remain for the future:

Challenges for Theory

1. How does the efficiency of particle acceleration affect the thermal properties of shocks? Can the efficiency be unambiguously derived from thermal X-ray diagnostics?
2. Amplification of magnetic field in efficient shocks: does it occur? To what extent?
3. Electron *injection* is still not understood. How might it depend on obliquity? (SN1006: are the two bright limbs polar caps, or sides of an equatorial barrel?)
4. Shock precursors are not yet seen, in particular synchrotron halos. Pre-acceleration of thermal gas should also produce broadening of the narrow component of Balmer lines in Ia remnants.
5. Non-thermal bremsstrahlung: models need to include post-shock Coulomb losses. Calculations need to be done on the effects of non-thermal bremsstrahlung on ionization and line excitation.

Challenges for Observations

1. Can we get better evidence for curvature of integrated radio spectra? Can spatial variations be detected with longer frequency baselines?

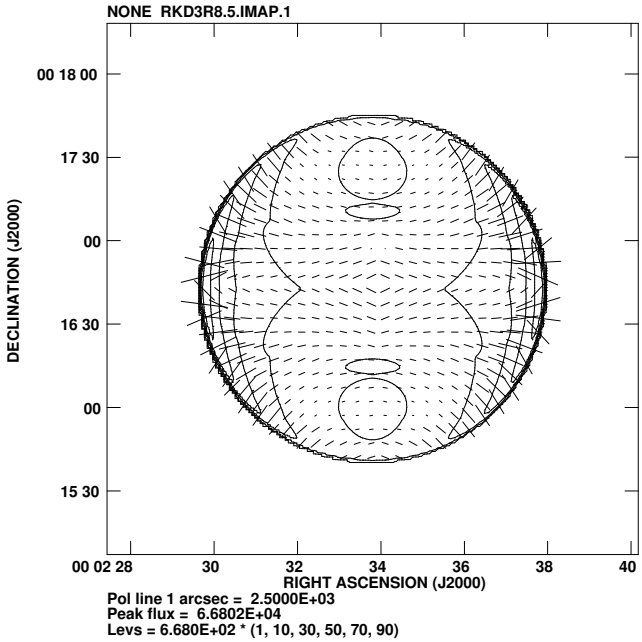

Figure 21: Polarization vectors at 300 MHz corresponding to Fig. 19.

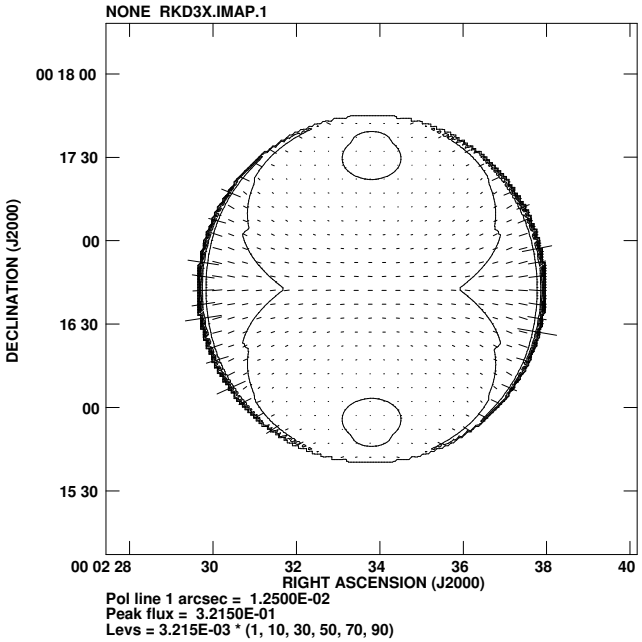

Figure 22: As in Fig. 21, for emission at 1 keV.

2. We should be routinely adding single-dish data to interferometer maps to eliminate missing-flux uncertainties.

3. High energy-resolution X-ray spectra are required to separate thermal and non-thermal continua (Astro-E 2 is on the way!).

4. X-ray polarimetry: can a successful mission be organized?

Acknowledgments

I thank the organizers of this interesting meeting for the opportunity to review important SNR physics. This work was supported in part by NASA Astrophysics Theory Program grant NAG5-7153.

References

Achterberg, A., Blandford, R. D., Reynolds, S. P. 1994, A&A, 281, 220

Badenes, C., Bravo, E., Borkowski, K.J., Domíguez, I. 2003, ApJ, 593, 358

Bamba, A., Yamazaki, R., Ueno, M., Koyama, K. 2003, ApJ, 589, 827

Becker, R. A., et al. 1980, ApJ, 240, L33

Berezhko, E. G., Ksenofontov, L. T., Völk, H. J. 2003, A&A, 412, L11

Blandford, R. D., Eichler, D. 1987, Phys.Rep. 154, 1

Blondin, J. M., Wright, E. B., Borkowski, K. J, Reynolds, S. P. 1998, ApJ, 500, 342

Blondin, J. M., Borkowski, K. J, Reynolds, S. P. 2001, ApJ, 557, 782

Borkowski, K. J., Lyerly, W. J., Reynolds, S. P. 2001, ApJ, 548, 820

Borkowski, K. J., et al. 2001b, ApJ, 550, 334

Butt, Y. M., et al. 2002, Nature, 418, 499

Chevalier, R. A. 1982a, ApJ, 258, 790

Chevalier, R. A. 1982b, ApJ, 259, L85

Cioffi, D. F., McKee, C. F., Bertschinger, E. 1988, ApJ, 334, 252

Dickel, J. R., Strom, R. G., Milne, D. K. 2001, ApJ, 546, 447

Dwarkadas, V., Chevalier, R. A. 1998, ApJ, 497, 807

Dyer, K. K., et al. 2001, ApJ, 551, 439

Ellison, D. C., Reynolds, S. P. 1991, ApJ, 382, 242

Ellison, D. C., Slane, P. O., Gaensler, B. M. 2001, ApJ, 563, 191

Enomoto, R., et al. 2002, Nature, 416, 823

Gaensler, B. M., Hendrick, S. P., Reynolds, S. P., Borkowski, K. J. 2003, ApJ, 594, L111

Ghavamian, P., et al. 2001, ApJ, 547, 995

Green, D. A. 2004, "A Catalogue of Galactic Supernova Remnants (2004 January version)", Mullard Radio Astronomy Observatory, Cavendish Laboratory, Cambridge, United Kingdom (available at

"http://www.mrao.cam.ac.uk/surveys/snrs/").
Hendrick, S. P., Reynolds, S. P. 2001, ApJ, 559, 903
Hendrick, S. P., Borkowski, K. J., Reynolds, S. P. 2003, ApJ, 593, 370
Jokipii, J. R. 1987, ApJ, 313, 842
Jones, F. C., Ellison, D. C. 1991, SpSciRev, 58, 259
Jun, B.-I., Jones, T. W. 1999, ApJ, 511, 774
Jun, B.-I., Jones, T. W., Norman, M. L. 1996, ApJ, 468, L59
Koyama, K., et al. 1995, Nature, 378, 255
Lazendic, J., et al. 2004, ApJ, 602, 271
Li, H., McCray, R., Sunyaev, R. A. 1993, ApJ, 419, 824
Long, K. S., et al. 2003, ApJ, 586, 1162
Lucek, S. G., Bell, A. R. 2000, MNRAS, 314, 65
Malkov, M. A., Drury, L. O'C. 2001, Rep, Progr. Phys., 64, 429
McKee, C. F. 1974, ApJ, 188, 335
Nadyozhin, D. K. 1985, ApSS, 112, 225
Park, S., et al. 2003, ApJ, 592, L41
Reynolds, S. P. 1996, ApJ, 459, L13
Reynolds, S. P. 1998, ApJ, 493, 375
Reynolds, S. P. 2004a, *Proc. 2002 Huntsville Workshop on Particle Acceleration in Geospace and Beyond*, in press.
Reynolds, S. P. 2004b, Adv. Space. Res., 33, 461
Reynolds, S. P., Chevalier, R. A. 1981, ApJ, 245, 912
Reynolds, S. P., Ellison, D. C. 1992, ApJ, 399, L75
Reynolds, S. P., Gilmore, D. M. 1986, AJ, 92, 1138
Reynolds, S. P., Keohane, J. W. 1999, ApJ, 525, 368
Rho, J., Petre, R. 1998, ApJ, 503, L167
Rho, J., Dyer, K. K., Borkowski, K. J., Reynolds, S. P. 2002, ApJ, 581, 1116
Slane, P.O., et al. 1999, ApJ, 525, 357
Vink, J., Kaastra, J. S., Bleeker, J. A. M. 1997, A&A, 328, 628
Vink, J., et al., in New Visions of the X-ray Universe in the *XMM-Newton* and *Chandra* Era (Noordwijk: ESA/ESTEC), in press
Wardle, M., Yusef-Zadeh, F. 2004, Science, 296, 2350
Whiteoak, J. B. Z., Green, A. J. 1996, A&AS, 118, 329
Woltjer, L. 1972, ARAA, 10, 129